Gas Bubble Nucleation and Migration in Soils—Pore-Network Model Simulation

Nariman Mahabadi[1], Xianglei Zheng[2], Tae Sup Yun[3], and Jaewon Jang[4(✉)]

[1] Arizona State University, Tempe, AZ, USA
[2] Municipal Testing Laboratory, New York, USA
[3] Yonsei University, Seoul, South Korea
[4] Hanyang University, Seoul, South Korea
jwj@hanyang.ac.kr

Abstract. Sediment can be de-saturated by introducing gas bubbles, which is found in various applications such as methane gas generation in landfill, microbial-induced gas bubble formation, air sparing method for soil remediation, heavy oil depressurization for carbon recovery, and gas production from hydrate bearing sediment. The gas introduction method (e.g., nucleation and injection) and migration and trapping of gas bubbles affect the hydraulic conductivity, residual gas saturation, and the stability of these gassy sediments. In this study, the pore-network model is used to investigate gas bubble migration in porous media. Gas bubbles are introduced by mimicking either nucleation or injection. Based on the known gas bubble behavior available in the literature, numerical algorithms are developed to simulate the migration and trapping of gas bubbles in pore-network model. The effect of gas bubble size distribution and pore size distribution on residual saturation is investigated. The results show that gas bubble size distribution becomes wider as gas bubbles coalesce to each other during migration. And the residual gas saturation increase with increasing bubble size and permeability reduction becomes apparent as the gas bubble size and the number of generated gas bubble increase.

1 Introduction

Soils can be de-saturated by several gas formation mechanisms such as microbial activity in shallow ocean sediments or wetlands, methanogenic degradation of hydrocarbon contaminants in the subsurface (Amos et al. 2005), decomposition of municipal solid waste in landfills (van Breukelen et al. 2003), air trapping by groundwater-level oscillation (Krol et al. 2011), and seasonal temperature variation resulting in gas solubility change in the subsurface (Ryan et al. 2000). In addition, there is a possibility of gaseous CO_2 formation by the leakage-induced depressurization of CO_2-dissolved brine during the long-term geological CO_2 sequestration (Plampin et al. 2014; Zuo et al. 2012; Zuo et al. 2013).

On the other hand, gas bubbles can be also introduced artificially to remediate contaminated soils, modify the properties of the sediments, and produce resources in various applications such as air sparging or gas exsolution by supersaturated water

S. Wang et al. (eds.), *New Solutions for Challenges in Applications of New Materials and Geotechnical Issues*, Sustainable Civil Infrastructures,
https://doi.org/10.1007/978-3-319-95744-9_3

injection (SWI) for soil remediation (Enouy et al. 2011; McCray and Falta 1997), denitrification and induced partial saturation (IPS) for liquefaction prevention (Eseller-Bayat et al. 2013; He and Chu 2014; Rebata-Landa and Santamarina 2012), heavy oil depressurization to reduce viscosity (e.g., solution gas drive) (Bora et al. 2000; Stewart et al. 1954), methane gas production from hydrate-bearing sediments (Jang and Santamarina 2011, 2014; Jang and Santamarina 2016), and CO_2 sequestration/CO_2 foam injection (Zheng and Jang 2016; Zheng et al. 2017). The gas generation mechanisms in the abovementioned applications include direct gas bubble injection, depressurization, temperature increase, electrolysis, and drainage-recharge.

Once the gas bubbles are generated in the sediment, they can migrate upward due to the buoyancy, or are sometimes trapped in the pore space. The gas nucleation, migration, and trapping and the associated effects are frequently found in the in situ sediment. Methane ebullition, the release of methane into the atmosphere or the movement through porous media, is the typical mechanism of greenhouse gas emission from aquatic ecosystems (Amos and Mayer 2006; Ramirez et al. 2015; Walter et al. 2006). Sometimes, methane bubbles burst out and form a crater in the permafrost gradually thawing due to the global warming (Moskvitch 2014). The gas bubble formation in the shallow ocean sediment also affects the mechanical properties of the sediment (Grozic et al. 1999; Sills et al. 1991). In addition, very small gas bubbles trapped in the porous media can dramatically reduce hydraulic conductivity without the significant reduction in water saturation (Ronen et al. 1989).

The initial size of gas bubbles upon nucleation, the coalescence of gas bubbles during migration, the bubble generation rate, and the pore throat size of the sediment could affect the behavior of gas migration and trapping in the porous media. In this study, we studied the behavior of gas bubble migration in the porous media and investigated the effect of gas bubble size on the residual gas saturation and hydraulic conductivity.

2 Simulation Details

The migration of gas bubbles through the porous media is simulated using the pore network model extracted from 3D X-ray CT image of soils. Several numerical algorithms and criteria for the size-dependent velocity of rising gas bubbles, bubble coalescence, escaping, and trapping in the pore space are summarized in this section.

2.1 Pore Network Model Extraction from X-Ray CT Image

A sediment core used for the X-ray scanning was recovered from Mallik 5L-38 site in Beaufort Sea, Canada (The grain size distribution of the sediment and the information on the X-ray scanning is available in Mahabadi et al. (2016a) and Mahabadi et al. (2016b). The volume of the scanned image is 27 mm^3 (3 mm × 3 mm × 3 mm) with 12.5 μm pixel resolution. The obtained CT images provide the three-dimensional structure of the scanned sediment, including both the grains and the pore spaces (Fig. 1a). Then, the maximal ball algorithm developed by Dong and Blunt (2009) is employed to extract the three-dimensional pore-network model from the X-ray CT

images (Mahabadi and Jang 2014; Mahabadi et al. 2016b) (Fig. 1a). The maximal ball algorithm generates spheres inscribed in the pore wall. Then, the bigger spheres turn into the pores of the pore-network model and the size of smaller spheres located in pore throats are used as the radii of cylindrical tubes connecting the neighboring pores. As a result, the pore-network model consists of the spherical pores connected by cylindrical tubes. The extracted pore network model consists of 4593 pores and 19361 tubes with the tube connectivity per pore (coordination number) of cn = 8.0. Figure 1b shows the pore and tube size distribution of the extracted pore network model.

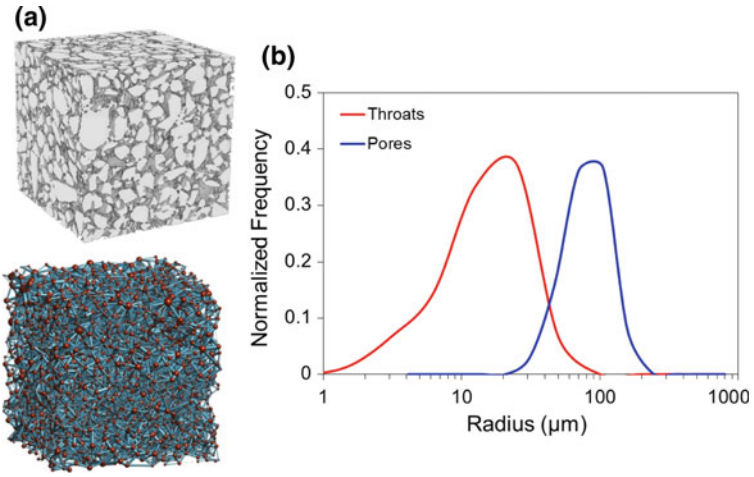

Fig. 1. Details of pore-network model simulation. (a) CT-Scan images from 3 mm × 3 mm 3 mm sample of Mallik Sand, and pore network model extracted from the CT-scan image. The extracted pore network model consists of 4593 pores and 19361 tubes with the tube connectivity per pore (coordination number) of cn = 8.0. Mean pore radius is $\mu[R_{pore}]$ = 69.3 μm, mean tube size is $\mu[R_{tube}]$ = 12.5 μm, and mean tube length $\mu[L_{tube}]$ = 45 μm ($max[R_{pore}]$ = 194 μm, $min[R_{pore}]$ = 22 μm, $max[R_{tube}]$ = 63 μm, $min[R_{tube}]$ = 1 μm). (b) Pore and throat size distribution.

2.2 Bubble Generation and Migration

Bubble generation. Gas bubbles are nucleated at randomly selected pores in the pore-network model. Only one gas bubble is generated per a pore. The ratios of the number of the nucleated gas bubbles N_B over the total number of pores N_P used in this simulation include N_B/N_P = 0.2, 0.4, 0.6, and 0.8. Regarding the bubble size, either (1) mono-sized bubbles are nucleated at the selected pores or (2) the sizes of bubbles are determined by the size of pores that occupy the bubbles. The size of mono-sized bubbles used in the simulation ranges from R_B = 5 μm to 80μm. And the ratio of the bubble radius R_B over the host pore radius R_P used in this study ranges from R_B/R_P = 0.125 to 0.5.

Rising bubble velocity. The velocity of a spherical solid particle settling in water is derived from the Stokes' law (ASTM 2016) in which the gravitational force of the particle is assumed to be the same as the viscous drag force by the fluid, resulting in the terminal velocity V_s [m/s]:

$$V_s = \frac{g(\rho_s - \rho_w)d^2}{18\mu} \tag{1}$$

where g[m/s^2] is the gravitational acceleration, ρ_s[kg/m^3] is the particle density, ρ_w[kg/m^3] is the water density, d [m] is the particle diameter, and μ[kg/(m s)] is the dynamic viscosity of the fluid. For the case of a gas bubble ascending in a fluid due to the buoyancy, the velocity of the rising bubble V_B in water can be estimated from Eq. 1 by assuming the mass density of the gas bubble to be zero.

As a gas bubble moves upward, it is expected that the bubble size increases due to the decreasing hydrostatic pressure. But, in this study, the size of the gas bubble is assumed to be constant due to the small change in hydrostatic pressure within a 3 mm in height of the pore network model [Note that the size of the air bubble increases 3%–5% while it moves along 1 m in vertical distance (Roosevelt and Corapcioglu 1998)]. Therefore, once a bubble nucleates, a constant velocity is assigned to the bubble.

Bubble migration, coalescence, and trapping. Once a gas bubble is assigned in a pore, the gas bubble migrates upward through one of the tubes connected to the pore. Consider a pore i P_i connected to neighboring pores j P_j through tube ij T_{ij}. For each pore j connected to the pore i, the following value is calculated:

$$\sin\theta = \frac{(z_j - z_i)}{L_{ij}} \tag{2}$$

where z_j and z_i are z-coordinates of P_i and P_j, and L_{ij} is the length of the tube ij T_{ij} connecting P_i and P_j. Therefore, sinθ means the vertical gradient of the tube along z-axis ($-1 \leq \sin\theta \leq 1$). All tubes connected to P_i are ranked based on sinθ values. It is assumed that the bubble migrates through the tube that has the highest sinθ value. If the tube has a negative sinθ value, the bubble will not migrate through the tube due to the buoyancy. Based on this criterion, the tube with highest sinθ-value is selected as the pathway for bubble migration unless the P_j or T_{ij} is blocked by a gas bubble. When the radius of the bubble inside P_i is greater than the radii of all T_{ij} connected to P_i, the gas bubble is considered as trapped in the pore. If there is a trapped gas bubble in a pore, another bubble could migrate into the pore and coalesces to the existing trapped gas bubble as long as the coalesced gas bubble size is smaller than the pore size.

A time step Δt_m is selected such that only one gas bubble (moving from P_i to P_j along the tube ij T_{ij}) is allowed to arrive at the neighboring pore j during the time step:

$$\Delta t_m = \min\left[\frac{\Delta L_{ij}}{v_{ij}}\right] \tag{3}$$

where v_{ij} is the velocity of the rising bubble in the tube ij T_{ij} connecting P_i and P_j and ΔL_{ij} is the distance from the gas bubble in the T_{ij} to the neighboring pore j P_j. Therefore, only one bubble can reach to the neighboring pore at each time step unless there is a coalescence between two bubbles in a tube.

The coalescence of gas bubbles can happen in the tube. Consider two gas bubbles, B_1 and B_2, migrating in the same tube. At the time $t = t_1$, the locations of small bubble

B_1 and large bubble B_2 are L_1 and L_2 from the input side (bottom) of the tube, respectively. The coalescence of the two bubbles occurs at the time $t = t_1 + \Delta t_c$ for the condition below,

$$(L_1 + V_1 \Delta t_c) - (L_2 + V_2 \Delta\, t_c) = R_{B1} + R_{B2} \tag{4}$$

where V_1 and V_2 are the velocity of the rising bubbles B_1 and B_2 which are dependent on the their sizes, and R_{B1} and R_{B2} are the radii of the bubble B_1 and B_2.

The time step for bubble coalescence Δt_c is calculated from Eq. 4:

$$\Delta\, t_c = \frac{L_1 - (L_2 + R_{B1} + R_{B2})}{V_2 - V_1} \tag{5}$$

The minimum coalescence time step Δt_c is chosen such that only one coalescence event is allowed to occur for all the bubbles moving in all the tubes. When the two bubbles are merged together and form a bigger bubble, the velocity of the merged bubble is calculated based on its new size. If the radius of the merged bubble is bigger than the radius of the tube, the gas bubble is considered to be trapped in the tube.

Once Δt_c is calculated, the smaller time step between Δt_m and Δt_c is chosen for the global time step $\Delta t = \min[\Delta t_m, \Delta t_c]$. Based on the calculated time step Δt, the location of the bubbles in the pore-network model is updated during the migration and this procedure is repeated until there is no further movement of gas bubbles in the pore-network model. During the migration, the bubbles arriving at the outlet pores in the top layer escape from the pore network model.

Hydraulic conductivity. Once a gas bubble is trapped in a pore, the tubes connected to the pore loose conductivity. Therefore, for the conductivity calculation, the pore and the neighboring tubes are removed from the pore network model assuming zero conductivity. At the end of each gas migration simulation, the hydraulic conductivity is calculated (Jang et al. 2011) and normalized by the hydraulic conductivity obtained for 100% water saturation condition.

3 Results and Analyses

In this study, the effect of bubble size on the gas bubble migration in the porous media is investigated. Two cases of the bubble size distribution are considered: (1) mono-sized bubbles, and (2) distributed-sized bubbles. The size of bubbles are varied from $R_B = 5$ μm to 65 μm for the mono-size bubble case. And for the distributed-size bubble case, the ratio of the bubble radius R_B over the host pore radius R_P varies from $R_B/R_P = 0.125$ to 0.5.

Gas bubbles are initially assigned to the randomly chosen pores such that each pore occupies only one bubble. The ratios of the number of pores that occupy gas bubbles over the total number of pores in the pore-network model are $N_B/N_P = 0.2$, 0.4, 0.6 and 0.8. The generated gas bubbles start migrating upward towards the outlet in the top layer due to the buoyancy. Some of gas bubbles are trapped in the pore-network model, which determines the final gas saturation after the simulation. Initial and final images

during gas bubble migration for mono-sized bubble case (R_B = 15 μm, N_B/N_P = 0.4) are shown in Fig. 2. During the bubble migration, a rising bubble can be merged with the bubble already trapped in the upper pore and form a bigger bubble.

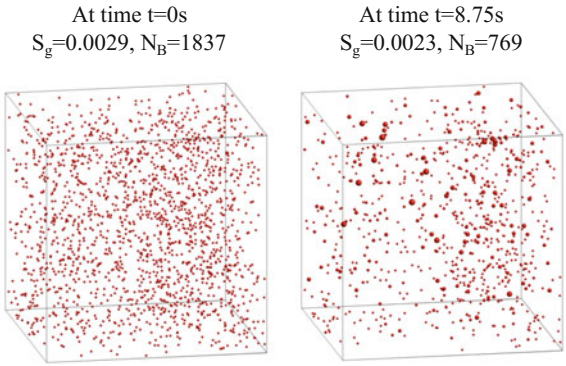

Fig. 2. Gas bubble location during gas migration and coalescence. Mono-size bubbles for bubble size R_B = 15 μm and N_B/N_P = 0.4 (N_B = 1837, N_P = 4593). Left column shows the initial nucleation of bubbles and the right column shows the final gas bubble saturation.

During gas bubble migration, some gas bubbles escape from the pore-network model when they reach to the top layer, some gas bubbles are trapped inside the pore-network, and some gas bubbles are coalesced to each other forming bigger gas bubbles. Therefore, the gas bubble size distribution changes and the number of total gas bubbles N_B decrease (Fig. 3). For mono-sized case, initially, there were a total of 1787 uniform-sized (R_B = 15 μm) gas bubbles. And there occur bigger gas bubbles during the simulation due to the coalescence and the size distribution curve becomes wider. The total number of gas bubble at the end of the simulation is N_B = 769. And for distributed-size case, the number of gas bubbles smaller than $R_B \sim 25$ μm decreases (possibly due to escaping and coalescence) and the number of gas bubbles larger than $R_B \sim 25$μm increases during the simulation.

The total migration time increases as the size of gas bubbles decreases regardless of the initial number of bubbles for mono-size bubble case study. In this case, all the bubbles move at the same ascending velocity as long as their sizes are the same (predicted by Eq. 1). As a result, the total migration time is only a function of the initial bubble size for a given pore network model dimension. However, the total migration time for distributed-sized bubble case also increases as R_B/R_P decreases. For distributed sized bubble case, the larger number of nucleated gas bubbles (higher N_B/N_P) results in wider bubble size distribution which means N_B/N_P = 0.8 case could include some bubbles smaller than the smallest bubble and larger than the largest bubble generated for the N_B/N_P = 0.2 case. For the low R_B/R_P ratio (e.g. R_B/R_P = 1/8), the smaller gas bubbles that have low ascending velocity require longer time to escape from the pore-network model. For the higher R_B/R_P ratio (e.g. R_B/R_P > 1/5), the large bubbles tend to block the pores and prevent the migration of bubbles, which reduces in total migration time.

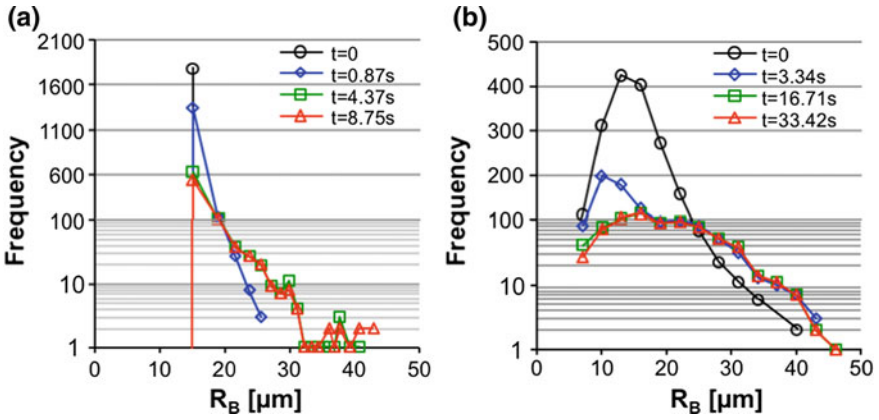

Fig. 3. Statistical and spatial bubble size distribution during gas bubble migration for the case of $N_B/N_P = 0.4$. (a) Mono-sized case (the initial size of gas bubble $R_B = 15$ μm). (b) Distributed-sized case (the ratio of pore size over bubble size $R_B/R_P = 1/5$). The change in gas bubble size distribution is shown during the migration due to coalescence.

If the radius of the bubble nucleated in a certain pore is bigger than the radii of any other tubes connected to the pore, the bubble is trapped in the pore. If another gas bubble migrates into the pore that occupies the trapped bubble, two gas bubbles are merged together and form a bigger trapped bubble as long as the volume of the coalesced gas bubble is smaller than the pore volume.

The residual gas saturations, the volume of trapped gas bubbles divided by the total volume of pore space, for mono-sized and distributed-size bubble cases are shown in first row in Fig. 4. The higher number of initial bubbles (higher N_B/N_P ratio) results in the higher residual gas saturation for a given bubble size.

When a gas bubble is trapped in a pore, the tubes connected to the pore loose the conductivity. Therefore, as more gas bubbles are trapped in the pore-network model, the global hydraulic conductivity of the pore-network model decreases. The hydraulic conductivity of the pore-network model with the trapped gas bubbles at the end of the simulation is normalized by the hydraulic conductivity of the pore-network model without the trapped gas bubbles for mono-sized and distributed-size cases (second row in Fig. 4). For the mono-sized case, the normalized hydraulic conductivity starts decreasing with increasing gas bubbles noticeably at the bubble radius $R_B = 20$μm which is near at the average of tube radius. For the case of the initial gas bubble radius larger than $R_B = 35$μm, the value of the reduced hydraulic conductivity is almost constant depending on the N_B/N_P ratio. Especially for the case of the mono-sized gas bubble larger than $R_B = 35$μm and $N_B/N_P = 0.8$ case, the hydraulic conductivity of the pore-network model at the end of the simulation becomes zero even at $S_r = 0.07$. For the mono-sized $R_B = 50$μm and $N_B/N_P = 0.2$ case, the hydraulic conductivity is reduced to 49% of the initial hydraulic conductivity at the very low gas saturation Sg = 0.07. However, for the distributed-sized case, the hydraulic conductivity at the end of the simulation is reduced gradually as the R_B/R_P ratio increases, and the reduced values becomes constant for the R_B/R_P ratio higher than $R_B/R_P = 0.33$.

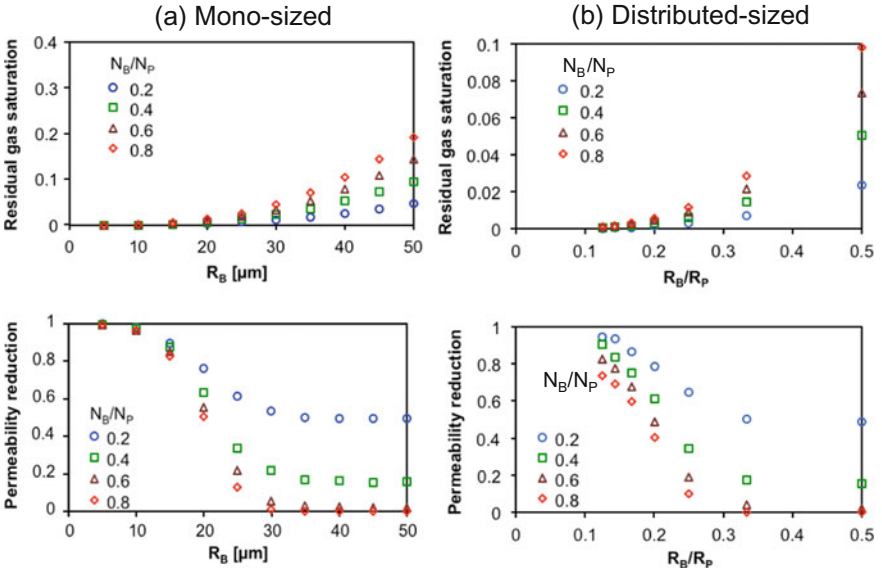

Fig. 4. Total migration time, trapped bubble fraction, residual saturation, and permeability reduction for (a) Mono-sized bubble migration and (b) Distributed-size bubble migration.

Relevance to in situ condition. In this study, all gas bubbles are generated instantaneously in the beginning of the simulation, and then the bubbles start migrating. However, the gas generation rate will be dependent on the in situ condition: The gas bubbles are generated very slowly via the natural microbial activity (Abrams 2005; Leifer and Patro 2002; Whalen 2005). The gas bubble generation by the denitrification process can be facilitated by injecting nutrient and controlling the environment such as the pH value of pore fluid (He and Chu 2014; Rebata-Landa and Santamarina 2012). Sometimes, gas bubbles can be generated very rapidly via the depressurization in the methane hydrate-bearing reservoir (Jang and Santamarina 2014).

The gas bubble generation rate and the initial gas bubble size upon nucleation can affect the gas bubble migration and the trapping. The gas bubble size upon nucleation and slow bubble generation rate (corresponding to the small R_B size and the low N_B/N_P case used in this study) will make it easier for gas bubbles to migrate upward without having coalescence and trapping. However, the large size of gas bubbles upon nucleation and rapid gas bubble generation rate (corresponding to the large R_B size and the high N_B/N_P case in this study) will facilitate the coalescence of gas bubbles and the possibility of trapping increases. Therefore, the in situ gas generation rate should be considered in order to apply the results of the pore-network model simulation to analyze the in situ gas bubble behavior.

The gas bubble movement (e.g., migration and trapping) through the porous media (which are in the sinusoidal shape consisting of wide pores and narrow pore throats) could be different than the gas bubble movement in the cylindrical tubes (Roosevelt and Corapcioglu 1998). A gas bubble whose size is equivalent to the pore size could migration and pass through the pore throat. Therefore, the pore-network model

simulation needs to be carefully used to understand the gas bubble behavior (e.g., gas bubble stability in pore space) at the in situ condition for a long-term prediction (e.g., effect of gas bubble formation on hydraulic conductivity and liquefaction prevention).

4 Conclusions

The coalescence of gas bubbles during the gas migration induces the change in the bubble size distribution. For both mono-sized and distributed-size cases, the bubble size distribution becomes wider and the total number of gas bubbles decreases during the simulation.

The residual gas saturation at the end of the simulation increases as the bubble size R_B for the mono-sized case and the R_B/R_P ratio for the distributed-sized case increases. This trend is more pronounced as the N_B/N_P ratio increases from $N_B/N_P = 0.2$ to 0.8. The hydraulic conductivity decreases due to the gas bubble trapping in the pore-network model. The hydraulic conductivity at the end of the simulation decreases as the gas bubble size R_B or the ratio R_B/B_P increases. The reduction of hydraulic conductivity is significant for the N_B/N_P ratio higher than 0.6: The hydraulic conductivity becomes zero for $R_B > 35\mu m$.

Finally, the gas bubble behavior and the associated property change obtained by the pore-network model simulation needs to be carefully used to predict the in situ gas bubble behavior due to the assumption used in this study.

Acknowledgements. This work was supported by the research fund of Hanyang University (HY-201700000002411).

References

Abrams, M.A.: Significance of hydrocarbon seepage relative to petroleum generation and entrapment. Mar. Pet. Geol. **22**, 457–477 (2005). https://doi.org/10.1016/j.marpetgeo.2004.08.003

Amos, R.T., Mayer, K.U.: Investigating ebullition in a sand column using dissolved gas analysis and reactive transport modeling. Environ. Sci. Technol. **40**, 5361–5367 (2006)

Amos, R.T., Mayer, K.U., Bekins, B.A., Delin, G.N., Williams, R.L.: Use of dissolved and vapor-phase gases to investigate methanogenic degradation of petroleum hydrocarbon contamination in the subsurface. Water Resour. Res. **41**(W02001), 02001–02015 (2005). https://doi.org/10.1029/2004WR003433

ASTM.: D7928-16 Standard test method for particle-size distribution (gradation) of fine-grained soils using the sedimentation (hydrometer) analysis, edited (2016)

Bora, R., Maini, B.B., Chakma, A.: Flow visualization studies of solution gas drive process in heavy oil reservoirs with a glass micromodel. SPE Reservoir. Eval. Eng. **3**(3), 224–229 (2000)

Dong, H., Blunt, M.: Pore-network extraction from micro-computerized-tomography images. Phys. Rev. E **80**(3), 0001 (2009). https://doi.org/10.1103/PhysRevE.80.036307

Enouy, R., Li, M., Ioannidis, M.A., Unger, A.J.A.: Gas exsolution and flow during supersaturated water injection in porous media: II Column experiments and continuum modeling. Adv. Water Res. **34**, 15–25 (2011). https://doi.org/10.1016/j.advwatres.2010.09.013

Eseller-Bayat, E., Yegian, M.K., Alshawabkeh, A., Gokyer, S.: Liquefaction Response of Partially Saturated Sands. I: Experimental Results. J. Geotechn. Geoenviron. Eng. **139**(6), 863–871 (2013). https://doi.org/10.1061/(asce)gt.1943-5606.0000815

Grozic, J.L., Robertson, P.K., Morgenstern, N.R.: The behavior of loose gassy sand. Can. Geotech. J. **36**, 482–492 (1999)

He, J., Chu, J.: Undrained Responses of Microbially Desaturated Sand under Monotonic Loading. J. Geotechn. Geoenviron. Eng. **140**(5), 04014003 (2014). https://doi.org/10.1061/(asce)gt.1943-5606.0001082

Jang, J., Santamarina, J.C.: Recoverable gas from hydrate-bearing sediments: Pore network model simulation and macroscale analyses. J. Geophys. Res. **116**(B8), 0001 (2011). https://doi.org/10.1029/2010jb007841

Jang, J., Santamarina, J.C.: Evolution of gas saturation and relative permeability during gas production from hydrate-bearing sediments: Gas invasion vs. gas nucleation. J. Geophys. Res. Solid Earth **119**(1), 116–126 (2014). https://doi.org/10.1002/2013jb010480

Jang, J., Santamarina, J.C.: Hydrate bearing clayey sediments: formation and gas production concepts. Mar. Pet. Geol. **77**, 235–246 (2016). https://doi.org/10.1016/j.marpetgeo.2016.06.013

Jang, J., Narsilio, G.A., Santamarina, J.C.: Hydraulic conductivity in spatially varying media-a pore-scale investigation. Geophys. J. Int. **184**(3), 1167–1179 (2011). https://doi.org/10.1111/j.1365-246X.2010.04893.x

Krol, M.M., Mumford, K.G., Johnson, R.L., Sleep, B.E.: Modeling discrete gas bubble formation and mobilization during subsurface heating of contaminated zones. Adv. Water Resour. **34**, 537–549 (2011). https://doi.org/10.1016/j.advwatres.2011.01.010

Leifer, I., Patro, R.K.: The bubble mechanism for methane transport from the shallow sea bed to the surface: A review and sensitivity study. Cont. Shelf Res. **22**, 2409–2428 (2002)

Mahabadi, N., Jang, J.: Relative water and gas permeability for gas production from hydrate-bearing sediments. Geochem. Geophys. Geosyst. **15**, 2346–2353 (2014). https://doi.org/10.1002/2014GC005331

Mahabadi, N., Zheng, X., Jang, J.: The effect of hydrate saturation on water retention curves in hydrate-bearing sediments. Geophys. Res. Lett. **43**(9), 4279–4287 (2016a). https://doi.org/10.1002/2016gl068656

Mahabadi, N., Dai, S., Seol, Y., Yun, T.S., Jang, J.: The water retention curve and relative permeability for gas production from hydrate-bearing sediments: pore-network model simulation. Geochem. Geophys. Geosyst. **17**, 3099–3110 (2016b). https://doi.org/10.1002/2016GC006372

McCray, J.E., Falta, R.W.: Numerical simulation of air sparging for remdiation of NAPL contamination. Ground Water **35**(1), 99–110 (1997)

Moskvitch, K.: Mysterious Siberian crater attributed to methane. Nature (2014). https://doi.org/10.1038/nature.2014.15649

Plampin, M., Illangasekare, T., Sakaki, T., Pawar, R.: Experimental study of gas evolution in heterogeneous shallow subsurface formations during leakage of stored CO2. Int. J. Greenhouse Gas Control **22**, 47–62 (2014). https://doi.org/10.1016/j.ijggc.2013.12.020

Ramirez, J.A., Baird, A.J., Coulthard, T.J., Waddington, J.M.: Testing a simple model of gas bubble dynamics in porous media. Water Resour. Res. **51**(2), 1036–1049 (2015). https://doi.org/10.1002/2014wr015898

Rebata-Landa, V., Santamarina, J.C.: Mechanical Effects of Biogenic Nitrogen Gas Bubbles in Soils. J. Geotech. Geoenviron. Eng. **138**(2), 128–137 (2012). https://doi.org/10.1061/(asce)gt.1943-5606.0000571

Ronen, D., Berkowitz, B., Magaritz, M.: The development and influence of gas bubbles in phreatic aquifers under natural flow conditions. Transp. Porous Media **4**, 295–306 (1989)

Roosevelt, S.E., Corapcioglu, M.Y.: Air bubble migration in a granular porous medium: Experimental studies. Water Resour. Res. **34**(5), 1131–1142 (1998). https://doi.org/10.1029/98wr00371

Ryan, M.C., MacQuarrie, K.T.B., Harman, J., McLellan, J.: Field and modeling evidence for a "stagnant flow" zone in the upper meter of sandy phreatic aquifers. J. Hydrol. **233**, 223–240 (2000)

Sills, G.C., Wheeler, S.J., Thomas, S.D., Gardner, T.N.: Behaviour of offshore soils containing gas bubbles. Geotechnique **41**(2), 227–241 (1991)

Stewart, C.R., Hunt Jr., E.B., Schneider, F.N., Geffen, T.M., Berry Jr., V.J.: The role of bubble formation in oil recovery by solution gas drives in limestones. J. Petrol. Technol. **5**(12), 21–28 (1954)

van Breukelen, B.M., Roling, W.F.M., Groen, J., Griffioen, J., van Verseveld, H.W.: Biogeochemistry and isotope geochemistry of a landfill leachate plume. J. Contam. Hydrol. **65**, 245–268 (2003). https://doi.org/10.1016/S0169-7722(03)00003-2

Walter, K.M., Zimov, S.A., Chanton, J.P., Verbyla, D., Chapin 3rd, F.S.: Methane bubbling from Siberian thaw lakes as a positive feedback to climate warming. Nature **443**(7107), 71–75 (2006). https://doi.org/10.1038/nature05040

Whalen, S.C.: Biogeochemistry of methane exchange between natural wetlands and the atmosphere. Environ. Eng. Sci. **22**(1), 73–94 (2005)

Zheng, X., Jang, J.: Hydraulic Properties of Porous Media Saturated with Nanoparticle-Stabilized Air-Water Foam. Sustainability **8**(12), 1317 (2016). https://doi.org/10.3390/su8121317

Zheng, X., Mahabadi, N., Yun, T.S., Jang, J.: Effect of capillary and viscous force on CO_2 saturation and invasion pattern in the microfluidic chip. J. Geophys. Res. **122**, 1634–1647 (2017). https://doi.org/10.1002/2016JB013908

Zuo, L., Krevor, S., Falta, R.W., Benson, S.M.: An Experimental Study of CO_2 Exsolution and Relative Permeability Measurements During CO_2 Saturated Water Depressurization. Transp. Porous Media **91**(2), 459–478 (2012). https://doi.org/10.1007/s11242-011-9854-2

Zuo, L., Zhang, C., Falta, R.W., Benson, S.M.: Micromodel investigations of CO_2 exsolution from carbonated water in sedimentary rocks. Adv. Water Resour. **53**, 188–197 (2013). https://doi.org/10.1016/j.advwatres.2012.11.004